water

MDPI

Article

Spatial and Temporal Variation of Droughts in the Mongolian Plateau during 1959–2018 Based on the Gridded Self-Calibrating Palmer Drought Severity Index

Yingchun Huang [1], Bowen Liu [1], Haigen Zhao [2,3,*] and Xudong Yang [1]

[1] Beijing Institute of Surveying and Mapping, Beijing 100045, China; huangyc@bism.cn (Y.H.); liubw@bism.cn (B.L.); yangxd@bism.cn (X.Y.)
[2] Chinese Academy of Agricultural Sciences, Institute of Environment and Sustainable Development in Agriculture, Beijing 100081, China
[3] Beijing Key Laboratory of Urban Spatial Information Engineering, Beijing 100045, China
* Correspondence: zhaohaigen@caas.cn

Abstract: Drought monitoring is challenging, but it is required for improving agricultural production, protecting the ecological environment, and reducing economic losses in drought-prone regions such as the Mongolian Plateau (MP). This study is a systematic analysis of the spatiotemporal changes in the characteristics of drought events (drought duration, severity, intensity, frequency, peak, and starting season) at the sub-regional scale between 1959 and 2018 based on the run theory and using the gridded self-calibrating Palmer Drought Severity Index (scPDSI) dataset. Principal component analysis and Varimax rotation and the Mann–Kendall trend and Sen's slope were used for the sub-regional division and drought trend analysis, respectively. In addition, wavelet analysis was employed to analyze drought periodicity and determine the influence of large-scale climate indices on regional drought variation. The study results indicate clear differences in the spatial patterns of drought characteristics in the MP. The northern part suffered from droughts with longer duration and higher severity, whereas more drought events with shorter duration and less severity occurred in the southern part. Most of the MP experienced a relatively wet trend in 1996–2018 compared to the period of 1959–1995. The frequency of spring drought events showed an increasing trend in 1996–2018, unlike in 1959–1995. Some drought events simultaneously affected two or several sub-regions. The wavelet analysis results indicated that the drought periodicity in the MP was 10–64 months. The Arctic Oscillation (Pacific Decadal Oscillation) was significantly correlated with drought in the southern (northern) part.

Keywords: drought monitoring; drought characteristics; scPDSI; run theory; drought trend and periodicity; Mongolian Plateau

Citation: Huang, Y.; Liu, B.; Zhao, H.; Yang, X. Spatial and Temporal Variation of Droughts in the Mongolian Plateau during 1959–2018 Based on the Gridded Self-Calibrating Palmer Drought Severity Index. *Water* **2022**, *14*, 230. https://doi.org/10.3390/w14020230

Academic Editors: Athanasios Loukas and Luis Gimeno

Received: 11 October 2021
Accepted: 4 January 2022
Published: 13 January 2022

1. Introduction

Drought is generally considered one of the most extreme weather events and it has a significant impact on ecosystems, agriculture, and the economy [1,2]. Drought was responsible for global annual losses of 221 billion dollars between 1960 and 2016 [3]. Moreover, the occurrence of drought is very complicated because of its long duration, high frequency, and widespread impact area [4]. Due to an increase in global warming, drought is occurring more and more frequently [5,6]. Therefore, drought monitoring is challenging, but it is required for improving agricultural production, protecting the ecological environment, and reducing economic losses.

In order to describe the characteristics and factors of drought more accurately, a number of drought indices have been developed and applied [7–11]. These drought indices can be roughly divided into two categories according to the method of establishment. One type of drought indicator is used to assess the statistical distribution of precipitation using

meteorological methods to reflect the intensity and duration of drought. Representative indicators of this type are the standardized precipitation index (SPI) [12] and the standardized precipitation evapotranspiration index (SPEI) [11]. Although these two indices have been used worldwide, they have certain disadvantages. The SPI index only considers the impact of precipitation, which is not consistent with the mechanism of drought and may result in a large error when characterizing drought. Compared with SPI, the SPEI does not only include the impact of precipitation but also considers the impact of potential evapotranspiration. However, Dai et al. [7] showed that it is the actual evapotranspiration and not the potential evapotranspiration that affects drought conditions. Additionally, potential evapotranspiration and actual evapotranspiration are often decoupled or even anticorrelated over many water-limited land areas [13].

In addition to statistical drought indices, the second type of drought indices is based on a definite physical meaning or a theory, e.g., the Palmer Drought Severity Index (PDSI) [10,14]. The PDSI is an estimate of standard soil moisture departure from normal conditions; it is calculated using a two-layer bucket hydrological model that considers the antecedent moisture supply, precipitation, and potential evapotranspiration. The PDSI synthetically takes into account changes in precipitation, evaporation, surface runoff, and soil water exchange and has been widely used to monitor and assess drought at a large scale in arid and semi-arid regions due to its insensitivity to temperature. The self-calibrating PDSI (scPDSI) [15] is based on the traditional PDSI and its empirical coefficients are adjusted according to the location and historical data at each site; therefore, the scPDSI is less constrained by region and has greater spatial comparability.

The main portion of the Mongolian Plateau (MP) includes the Inner Mongolia Autonomous Region and Mongolia. The area plays a significant role in the East Asian ecosystem and in the global carbon cycle [16,17]. Moreover, the arid and semi-arid natural environment of the MP results in high sensitivity to climate change [18]. With increasing global warming, the warming rate in the MP has exceeded the global warming rate [19]. Although the drought trend is increasing, there is a lack of drought research in the whole MP [3] compared to similar research in Inner Mongolia [20–24]. Gridded data are commonly appropriate for this type of research because they provide continuous spatial data when characterizing drought evolution in comparison with station-based data [25,26]. For example, Cao et al. [27] and Bao et al. [28] used normalized difference vegetation index (NDVI) and meteorological data for a 30-year period (1981–2011) to investigate the spatiotemporal dynamics of summer drought and the relationship with net primary productivity in the growing season in the MP. It is necessary to conduct long-term studies to analyze drought characteristics in the MP. Moreover, the sub-regional drought research is significant for analyzing the drought evolution in the whole region [26]. However, the previous studies had limited concern for the sub-regional drought change in MP. Additionally, it is crucial to understand the duration, frequency, intensity, and severity of drought events for developing policies to reduce the hazards of drought. Most studies have used only drought indices, e.g., SPEI and SPI, to analyze regional drought and did not investigate changes in the drought characteristics of the drought events.

Therefore, the objective of this study was to conduct a systematic analysis of the spatiotemporal changes in drought characteristics in the MP at the sub-regional scale using the gridded scPDSI index for the period of 1959 to 2018. The remainder of this paper is organized as follows: Section 2 introduces the study area and analysis method, and Section 3 presents the study results, including the sub-regional division based on a principal component analysis (PCA) and Varimax rotation method, the drought event extraction, and the drought characteristics obtained from the run theory. The Mann–Kendall (MK) trend test and Sen's slope are used for the drought trend analysis and wavelet analysis is used to determine the drought periodicity and the influence of large-scale climate indices on regional drought variation. Section 4 provides the discussion and Section 5 is the conclusion.

2. Data and Methods

2.1. Study Region

The MP is located in the interior of the Eurasian continent and includes the Inner Mongolia Autonomous Region of China and Mongolia [29]. The area is located between 87°40′–122°15′ E and 37°46′–53°08′ N (Figure 1). The main types of landforms are high plains and mountainous areas. The MP rises from the Great Hinggan Mountains in the east to the Altai Mountains in the west. The northern boundary is the Sayan Mountains and the Yabronov Mountains, and the southern boundary is the Yinshan Mountains. The area has a temperate continental climate and is the source of cold weather in the Asian continent. The region is characterized by short, hot summers and long, cold winters. The annual precipitation in most areas is less than 200 mm but reaches 400 mm in some mountainous areas. The precipitation mostly occurs in July–August, accounting for 75% of the annual precipitation [30]. The vegetation cover decreases from the northeast to the southwest, changing from forest to farmland, to grassland, and to desert [31]. The land cover includes desert, desert steppe, typical steppe, and meadow steppe.

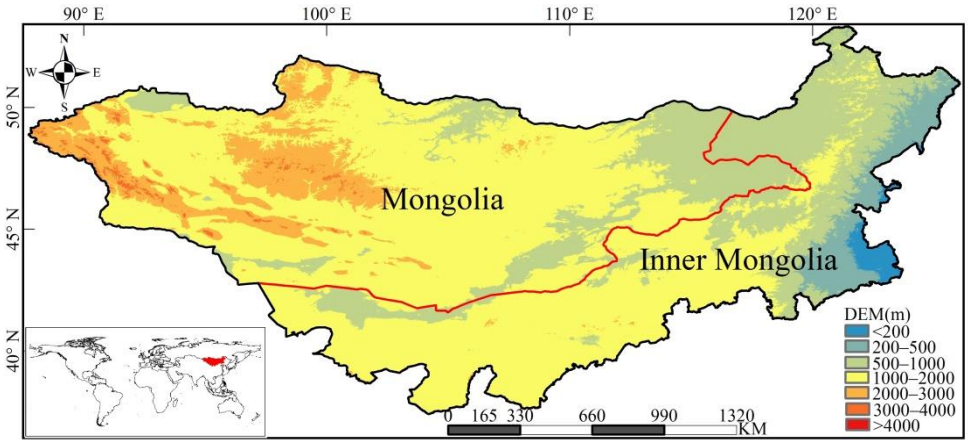

Figure 1. Geographical location and elevation in the Mongolian Plateau.

2.2. Data Sources

2.2.1. scPDSI Dataset

The scPDSI is based on the original PDSI developed by Palmer [10]; its objective is to be able to compare results from different climate regimes. In this study, the monthly scPDSI with a spatial resolution of 0.5° × 0.5° for global land is used and can be downloaded at https://crudata.uea.ac.uk/cru/data/drought/ (The last accessed date is 22 November 2021). The time series of precipitation and temperature to calculate the scPDSI were obtained from the latest version of the Climatic Research Unit (CRU) TS Version 4.03. More details on the scPDSI can be found in Wells et al. [15]. The monthly scPDISI dataset covers the period of 1901–2018. The scPDSI dataset is well-suited to characterize drought because the precipitation and temperature data provided by CRU are generated using a large number of global observation stations and the data underwent quality control [32]. Moreover, Wang et al. [24] has shown that the CRU dataset provided satisfactory results in Inner Mongolia. Because the number of stations used to generate the CRU dataset was limited prior to 1960 [33], the time period considered in this study is 1959 to 2018 (60 years). The drought categories of the scPDSI are listed in Table 1.

Table 1. Drought categories according to scPDSI values.

scPDSI Value	Category
≥4	Extremely wet
3 to 4	Severely wet
2 to 3	Moderately wet
1 to 2	Mildly wet
−1 to 1	Near normal
−2 to −1	Mildly dry
−3 to −2	Moderately dry
−4 to −3	Severely dry
≤−4	Extremely dry

2.2.2. Climate Indices

Previous studies [34–38] have reported that large-scale atmospheric circulation indices such as the Pacific Decadal Oscillation (PDO), Northern Arctic Oscillation (NAO), Arctic Oscillation (AO), and El Niño Southern Oscillation (ENSO) have an influence on the climate in the MP. In this study, wavelet coherence (WCO) analysis was used to determine the influence of large-scale climate patterns on regional drought variation. Detailed descriptions of the climate indices are listed in Table S1.

2.3. Methods

2.3.1. scPDSI

The PDSI [10] is based on the concept of the water balance equation under climatically appropriate for existing conditions. It shows the severity of drought in a period when the water supply in an area is continually below normal. It inputs time series of temperature and precipitation together with parameters related to the surface/soil characteristics into a two-layer bucket-type model for soil moisture computation [39]. The Palmer drought index formula is determined [10]:

$$X_i = Z_i/3 + 0.897X_{i-1} \tag{1}$$

where 1/3 and 0.897 are called persistence factors, X_{i-1} is the PDSI drought index of the last month, X_i is the PDSI drought index of the current month, and Z_i is the moisture anomaly index of the current month.

The scPDSI was developed based on the original PDSI to make the results of different climate regimes more comparable [15]. The improvement of scPDSI is how to calibrate the climate characteristic coefficient K value. The PDSI uses the following equations to obtain the *K* value [10]:

$$K = \left(\frac{17.67}{\sum_{1}^{12} \overline{D}K'}\right)K' \tag{2}$$

$$K' = 1.5 \cdot \log_{10}\left[\frac{\frac{\overline{PE}+\overline{R}+\overline{RO}}{\overline{P}+\overline{L}} + 2.8}{\overline{D}}\right] + 0.5 \tag{3}$$

where $\overline{D}$ is the average moisture departure, $\overline{L}$ is the average moisture loss of soil, $\overline{P}$ is the average precipitation, $\overline{RO}$ is the average runoff, $\overline{R}$ is the average moisture supply of soil, $\overline{PE}$ is the average potential evapotranspiration, and 17.67 is an empirical value.

As for scPDSI, fc, indicating the possibility of extreme drought, is considered and set as 0.2. The climate characteristic is calculated as [15]:

$$K = \begin{cases} K'(-4.00/2nd \quad percentile), & if \quad D < 0 \\ K'(4.00/98th \quad percentile), & if \quad D \geq 0 \end{cases} \tag{4}$$

This self-calibrating method uses fc and the original Palmer index to correct K and reflects the relationship between the studied climate region and the defined PDSI perimeter.

2.3.2. Identification of Drought Event Characteristics

The run theory is commonly employed to monitor and characterize the occurrence and evolution of drought events [40]. A specific time period in which the values of one variable are less than a selected threshold is considered a run [41]. As described by Guo et al. [26], a drought event was defined as the period (at least three months) in which the scPDSI was continuously negative, and the lowest srPDSI value was below −2 in this study. The reason is that a continuous low-intensity drought (scPDSI is larger than −2 and lower than 0) may result in significant damage to vegetation growth, agriculture, and the environment [42,43]. Moreover, by using this definition of a drought event, the accuracy of drought early warning systems is improved. The drought characteristics, such as the drought duration (DD), drought intensity (DI), drought frequency (DF), drought peak (DP), drought severity (DS), and drought event number (DEN), are defined according to the run theory (Figure 2). The drought duration is defined as the number of months of a drought event. The drought severity is the sum of the absolute scPDSI values in a drought event. The drought intensity is the drought severity divided by the drought duration. The drought peak represents the absolute lowest scPDSI during the drought event. The drought frequency refers to the reciprocal of drought interval, i.e., the mathematical inverse of the number of months between adjacent drought events [44]. The drought event number is the total number of drought events in a given period.

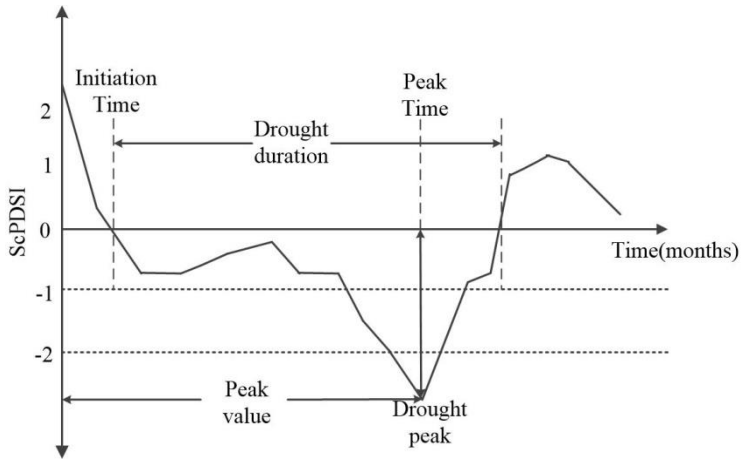

Figure 2. The sketch map of drought event definition and characteristics based on the run theory.

In order to characterize the temporal and spatial variation of drought events, the gridded annual mean drought duration, mean drought severity, mean drought intensity, and mean drought peak were calculated for each drought event (Equations (5)–(8)). In addition, the drought frequent season significance (DFSS) [20] was calculated by dividing the drought occurrence number in a given season by the number of all drought events. The DFSS can be used to monitor the effects of regional drought mitigation by judging the different seasons when drought events occur; 50% was used as the threshold in this study. The drought area (DA) was also calculated to characterize the spatial characteristics of drought events. The drought area is the ratio of the grids with drought characteristics and the total grid number in the study area.

$$MDD = \frac{\sum_{i=1}^{N} DD_i}{N} \quad (5)$$

$$MDS = \frac{\sum_{j=1}^{N} DS_j}{N} \; DS = \sum_{i=1}^{DD} |scPDSI_i| \quad (6)$$

$$MDI = \frac{\sum_{j=1}^{N} DI_j}{N} \; DI = \sum_{i=1}^{DD} |scPDSI_i| / DD \quad (7)$$

$$MDP = \frac{\sum_{j=1}^{N} DP_j}{N} \; DP = max|scPDSI_j|, 1 \le i \le DD \quad (8)$$

where i is the month of the drought event; DD, DS, DI, and DP have been defined earlier. N represents the number of drought events and j is one drought event.

The differences between the mean drought duration (MDD), mean drought frequency (MDF), mean drought severity (MDS), mean drought intensity (MDI), and mean drought peak (MDP) in 1959–1995 and those in 1996–2018 are the "relative differences in the annual mean drought duration" (abbreviated as RMDD), "relative differences in the annual mean drought frequency" (abbreviated as RMDF), "relative differences in the annual mean drought severity" (abbreviated as RMDS), "relative differences in the annual mean drought intensity" (abbreviated as RMDI), and "relative differences in the annual mean drought peak" (abbreviated as RMDP); these indices are used for a quantitative analysis of the drought characteristics.

2.3.3. Sub-Regional Division

In this study, the sub-regions were divided based on the similar drought co-variability of scPDSI using PCA. PCA is a mathematical transformation method used for dimensionality reduction and can distill structural information and extract patterns with similar variance characteristics. It transforms the original variables into several new uncorrelated principal components (PCs) to explain most of the total variance in original data based on the computation of the covariance matrix with the corresponding eigenvalues and eigenvectors [45]. The normalized eigenvectors, which are also called "loadings", represent the correlation between the original data and the time series of component scores. The number of PCs is decided based on the rule of thumb [46] and the scree plot, as well as the cumulative proportion of variance explained by PCs.

Otherwise, the Varimax rotation method was used to rotate the selected PCs to maximize the variance of the squared correlations and obtain a more stable localized drought pattern. The Varimax rotation can further maximize the variance of squared correlations between the rotated principle components (RPCs) and the variables and simplify the spatial patterns with similar temporal variations. In this study, 0.7 was chosen as the threshold of the sub-regional division.

2.3.4. Mann–Kendall Test and Sen's Slope

Linear regression methods require that the time series data are normally distributed, and these methods are susceptible to noise interference. In this study, the MK trend test [47,48] and Sen's slope [49] were used to determine the monthly scPDSI trends and the significance. The MK test is a non-parametric method and is used to determine the significance of trends in time series data [50,51]. In addition to trend analysis, the MK test has also been used to investigate abrupt changes in the standardized precipitation-evapotranspiration index (SPEI) time series [52]. Sen's slope uses the median of the slopes of several lines through pairs of points to fit a line to the sample data and was suitable for calculating the true slope of the MK trend line [53,54]. The drought event characteristics in Section 2.3.2 were compared in two periods that are separated by the abrupt changed year.

2.3.5. Wavelet Analysis

Wavelet analysis theory is based on the Fourier analysis method. Wavelet analysis can identify and describe the dominant localized variations in time series by decomposing data into time and frequency space [55]. The continuous wavelet transform (CWT) and the wavelet coherence (WCO) [56] were used to analyze the drought periodicity and the teleconnection between drought variation and large-scale climate patterns in this study, respectively. The continuous wavelet transform can express the high common power and the phase relationship during drought variation, while the wavelet coherence can be used to show the local high correlation between the drought variation and the climate indices. The wavelet analysis used the Morlet mother wave because of its reasonable localization [55]. For WCO, the phase relationship between two time series inputs (climate indices and scPDSI) is performed using directional arrows: the right and left arrows indicate in phase and anti-phase, respectively; the up (down) arrows imply climate indices leading (backward) scPDSI by 90°.

2.3.6. Local Regression

Local regression (LOESS) is a nonparametric smoothing operator which could be employed to explore the data change characteristics by capturing salient features that might be not featured in the original dataset [57,58]. It could be used to find the trend in datasets with missing data and obvious seasonality [59]. It could employ a function, which introduces minimal distortion into data boundaries, of the independent variable locally to smooth the dependent variable [57]. This type of smoothing function introduces minimal distortion into data boundaries, while presenting a simple design, straightforward use, and easy computer implementation. In this study, the local regression is specially designed to reveal the temporally linear trend for the monthly scPDSI in the MP and the six sub-regions.

3. Results

3.1. Sub-Regional Division

Based on the PCA and the Varimax rotation method, scPDSI was used to identify the sub-regional drought patterns. The Varimax rotation method indicated that the cumulative percentage of the first six PCs exceeded 70%. Table S2 shows the variance contributions of the un-rotated and rotated components based on monthly scPDSI. Based on the rule of thumb and the scree plot of eigenvalues, the MP was divided into six sub-regions (Figure 3), namely the northeast (NE), the southern MP (SM), the northwest (NW), the northern MP (NM), the southeast (SE), and the southwest (SW). In the following sections, the characteristics of drought could be analyzed in each sub-region.

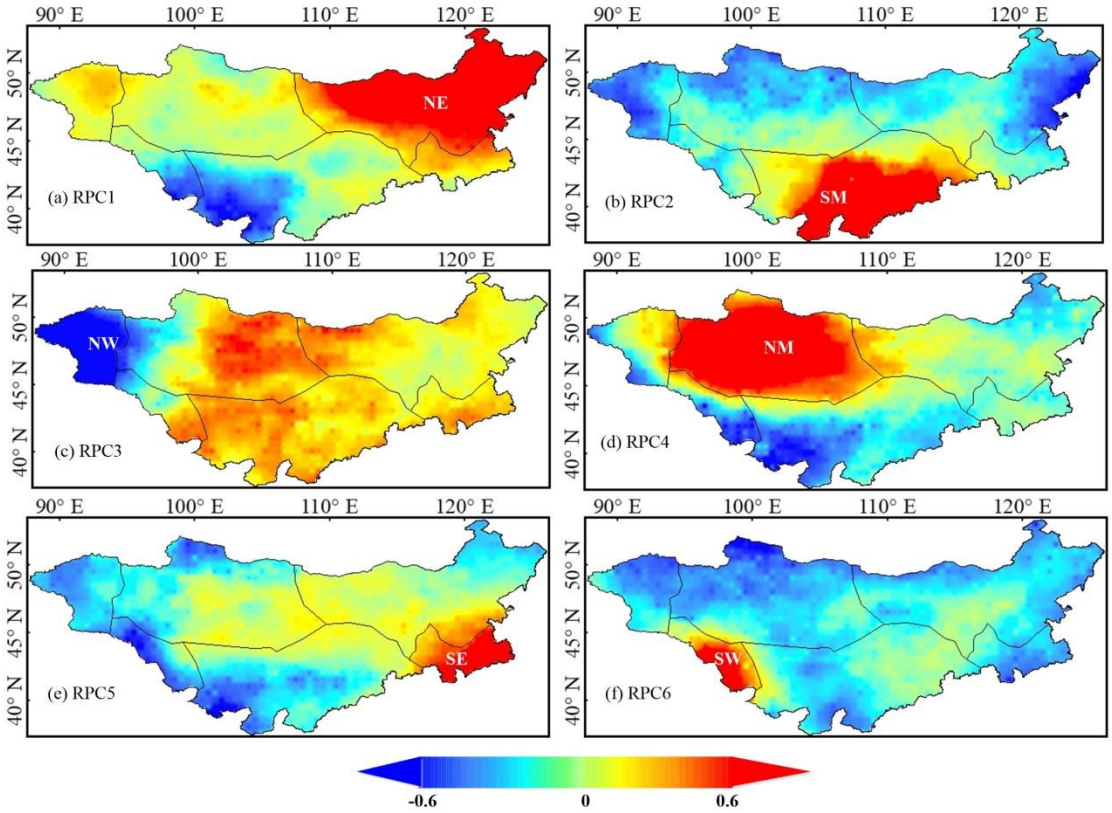

Figure 3. The sub-regional division based on the first six Varimax rotated components generated by PCA of the scPDSI. (**a**) RPC1, (**b**) RPC2, (**c**) RPC3, (**d**) RPC4, (**e**) RPC5, (**f**) RPC6.

3.2. Drought Characteristics Analysis

3.2.1. Drought Trend Analysis

The abrupt changes in the time series scPDSI based on the MK test and Sen's slope over the whole MP are shown in Figure 4a and Table S3. The red curve represents the sequential time series values, and the black curve denotes the backward sequence of the time series. If the intersection of the red curve and black curve is below the threshold value at a given significance level, it represents an abrupt change in the time series data [3]. In Figure 4a, 1976 and 1995 are two abrupt changes at the significance level of 0.05 with a threshold of ± 1.96.

Figure 4b shows the annual spatially averaged scPDSI in the whole MP (black solid line). A decreasing trend of the scPDSI is observed from 1959 to 2018 and the rate of decrease is -0.0280/yr. The annual average scPDSI values in 1959–1976, 1976–1995, and 1996–2018 (red solid lines) exhibit slight differences (1959–1976 (0.22) and 1976–1995 (-0.14)). However, there is a noticeable decreasing drought trend from 1996 to 2018, and the average value is -1.04. The results in Figure 4a,b indicate that 1995 was the year with the most abrupt change in the scPDSI in the past 60 years in the MP. Furthermore, a similar result has been achieved in Figure 5 based on the Pettitt test [60].

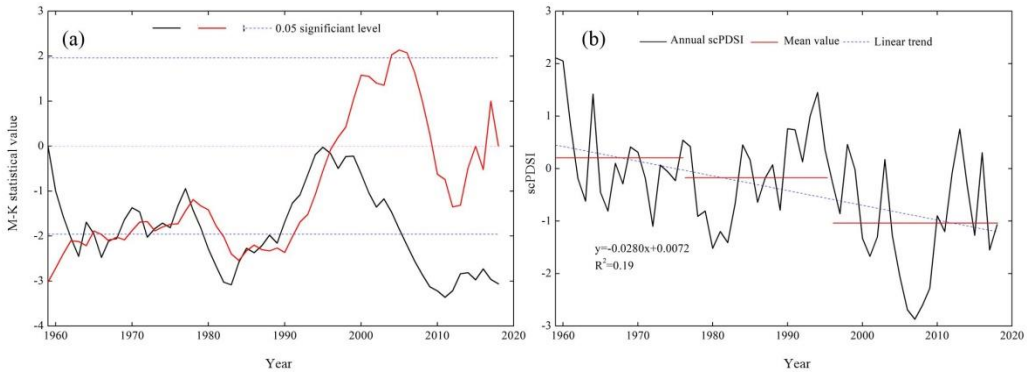

Figure 4. Abrupt changes (**a**) and annual trend (**b**) based on the scPDSI in the whole Mongolian Plateau from 1959 to 2018.

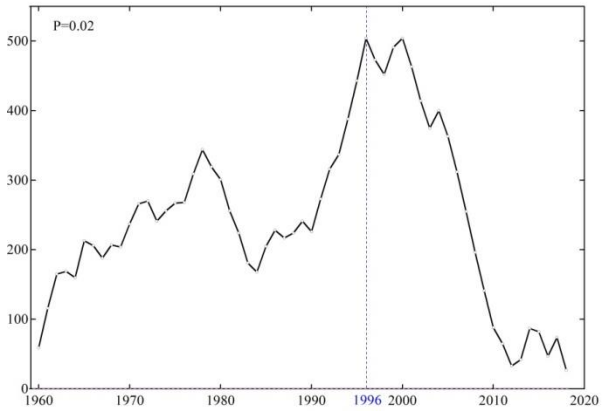

Figure 5. Abrupt changes based on the Pettitt test about the scPDSI in the whole Mongolian Plateau from 1959 to 2018.

3.2.2. Temporal Characteristics

The time series of the spatially averaged scPDSI values in the six sub-regions provide insights into the drought trend at the sub-regional scale. Figure 6 shows the monthly scPDSI in the MP and the six sub-regions, the linear trend, and the local regression (LOESS) curve for a 20-year period. The results indicate linear and nonlinear trends of the scPDSI.

All sub-regions exhibited a decreasing linear trend with different levels in the period 1959–2018 with the exception of the NW, which showed a wet trend. The 20-year LOESS curves indicate that the NE, SW, NM, SE, and NW experienced wetness with relatively higher scPDSI values in the 1990s. The NE, SE, and SW suffered from dryness in the 1960s to the 1980s. It is worth noting that all sub-regions suffered dryness after 2000 and the SE, SM, SW, and NM exhibited wetness trends after 2008.

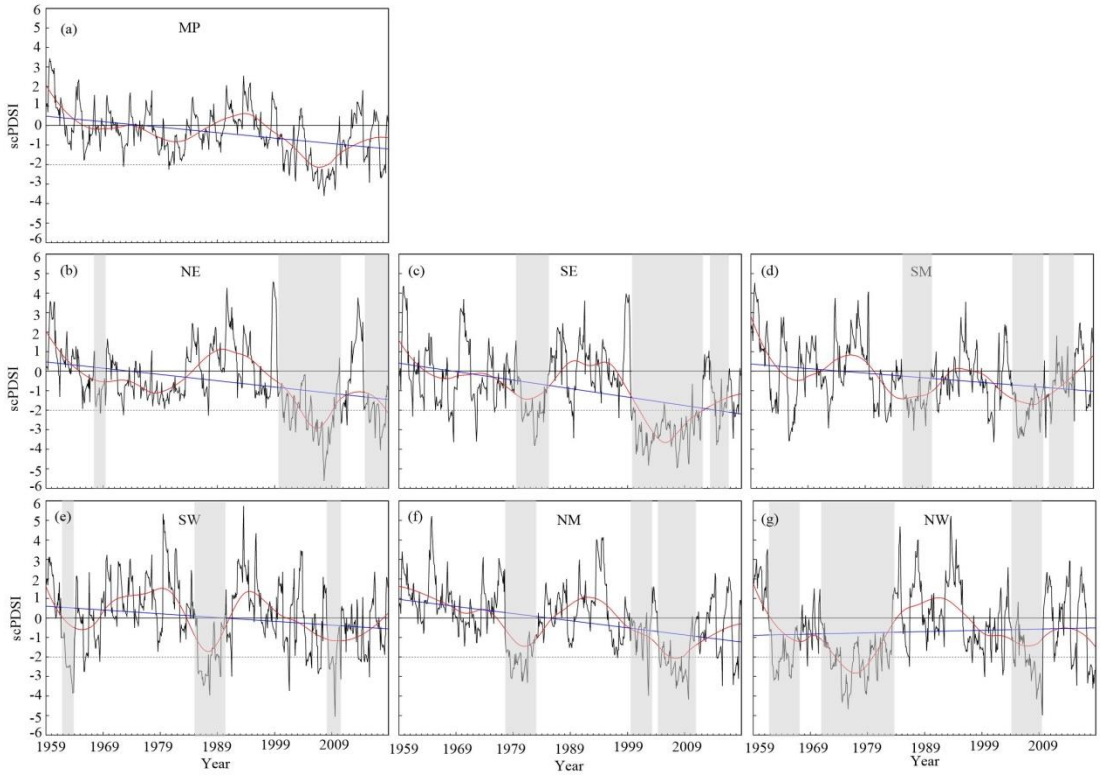

Figure 6. Evolution of the average scPDSI in the MP and the six sub-regions. The blue line represents the linear trend. The red line indicates the LOESS lines with a time span of 20 y. The gray areas represent the three drought events with the longest duration in the different sub-regions. (**a**) MP, (**b**) NE, (**c**) SE, (**d**) SM, (**e**) SW, (**f**) NM, (**g**) NW.

The quantitative results of the MK significance test and Sen's slope based on the regionally averaged scPDSI values are listed in Table 2. The results for 1959–2018 are consistent with the global linear trend displayed in Figure 6. The scPDSI in the NW region had positive slopes (0.62×10^{-3} and 1.03×10^{-3}) in 1959–2018 and 1996–2018, respectively (0.1 significance level). The larger slope values in 1996–2018 than in 1959–2018 implied that the NW underwent a persistent wet period in the past 60 years and the wetting trend became more pronounced after 1996. In contrast to the NW, the NE and SW suffered dry periods in 1959–2018 (-2.95×10^{-3} for NE and -1.80×10^{-3} for SW) and 1996–2018 (-2.92×10^{-3} for NE and -3.69×10^{-3} for SW) (0.01 significance level). The slope value for the NE in 1959–2018 was slightly different from that in 1996–2018 but the slope value for the SW was significantly lower in 1959–2018 than in 1996–2018; this indicates that the dry trend in the NE was stable over the past 60 years and the SW had a more pronounced dry period after 1996. Unlike the NE, SW, and NW, Table 2 shows that the slope values for the SE, SM, and NM are inconsistent during 1959–2018 (-3.51×10^{-3} for SE, -1.80×10^{-3} for SM and -3.17×10^{-3} for NM) and 1996–2018 (2.57×10^{-3} for SE, 0.20×10^{-3} for SM and 0.97×10^{-3} for NM) (0.01 significance level). Although the SE, SM, and NM experienced a dry trend in the past 60 years, a wetting trend was observed during 1996–2018, especially in the SE.

Table 2. The slopes of the lines of the spatially averaged scPDSI values in the six sub-regions in 1959–2018 and 1996–2018. The values are on a scale of 10^{-3}.

	NE	SE	SM	SW	NM	NW
1959–2018	−2.95 ***	−3.51 ***	−1.92 ***	−1.80 ***	−3.17 ***	0.62 *
1996–2018	−2.92 ***	2.57 ***	0.20 ***	−3.69 ***	0.97 ***	1.03 *

*, and *** indicate significant differences at the 0.1, and 0.01 level, respectively.

The drought area is also an important indicator that has been used to assess drought severity. Figure S1 in Supplementary Materials shows the temporal evolution of the areas suffering from moderate, severe, and extreme droughts based on the categories in Table 1 and method of drought area definition in Section 2.3.2. The SE, SM, SW, and NM had relatively higher drought area percentages in the 1980s and 2000s and higher drought area percentages were observed for the NE and NW in the 1970s and 2000s. It is worth noting that the drought area percentage in the NW had lower fluctuations after 2000, which is in agreement with the report that northwestern China has become wetter since the 1990s [37]. Although a relatively higher drought area percentage was observed after 1996, a noticeable decrease in the drought area percentage occurred after 2010 in the SE, SM, and NM, which is consistent with the results in Figure 4 and Table 2.

3.2.3. Typical Drought Events

Table 3 lists the most severe drought events with a duration >20 months in the six sub-regions; the drought characteristics were calculated using the spatially averaged scPDSI value. Some of the drought events are also depicted in Figure 6. These drought events are sorted by the values of drought severity.

In general, the number of severe drought events did not differ much for the period of 1959–1995 and 1996–2018. The drought events in 1960–1965 occurred mostly in the NW, SW, SM, SE, and NE and in 1970–1985 in the SE, SW, NM, and NW; in 2000–2012, these events occurred in all sub-regions. Moreover, the ranking of the drought severity was similar to that of the drought duration in the six sub-regions, which may be attributed to the atmospheric circulation anomalies that result in drought [61], such as Northern Arctic Oscillation, Arctic Oscillation, Pacific Decadal Oscillation (PDO), and Niño 3.4. Longer atmospheric circulation anomalies cause longer drought duration and greater drought severity. In addition, it is worth noting that the results for the drought area are not in good agreement with those of the drought severity and drought duration; the reason may be the underlying mechanism resulting in the occurrence of drought (e.g., anomalous high-pressure ridges or storm tracks).

Some drought events occurred simultaneously in two or several sub-regions. For example, the most severe drought events (yellow in Table 3) occurred in the NE and SE and lasted from 1999 to 2012, and the drought peak was September 2007. This drought event had a duration of 155 months and affected areas in the NE and SE (DAs of 81.14% and 95.22%, respectively). Additionally, the drought intensity in these two sub-regions was 2.09 and 3.04. In fact, this drought event extended to the SM and NM sub-regions. In these two sub-regions, the drought event lasted for about 3 years and the drought area values were 74.54% and 63.28%. Additionally, a severe drought event deserves special mention; it lasted from 1961 to 1969 and ranged from west to east (the drought peak was 1962 in NW, 1963 in SW, 1965 in SM, 1968 in NE, and 1968 in NE) across the MP and the drought intensity ranged from 1.19 to 2.26. Previous reports have demonstrated that such long-term and large-scale severe drought events cause great damage to agriculture and the economy in arid and semi-arid regions [26].

Table 3. Drought characteristics of typical drought events with durations >20 months occurring in the six sub-regions from 1959 to 2018. The green color represents drought events occurring in the time period of 1996–2018 in the six sub-regions. Dx represents the drought event, and the x shows the most severe drought events in six sub-regions. The smaller the number, the more serious the drought event.

Region	Event	Initiation Time	Peak Time	Termination Time	DD (Months)	DP	DS	DI	DA (%)
NE	D1	1999.07	2007.09	2012.05	155	−5.61	324.48	2.09	81.14
	D2	2014.07	2017.07	2018.12	54	−4.04	112.14	2.08	89.95
	D3	1967.08	1968.07	1969.07	24	−2.16	28.45	1.19	74.37
SE	D1	1999.07	2007.09	2012.05	155	−4.96	470.69	3.04	95.22
	D2	1979.10	1982.10	1985.05	68	−3.83	124.58	1.83	86.74
	D3	2013.08	2014.08	2016.10	39	−3.78	68.61	1.76	85.19
	D4	1971.08	1972.08	1974.06	35	−3.59	43.51	1.24	82.1
	D5	1967.08	1968.08	1969.06	23	−3.63	38	1.65	77.55
	D6	2016.12	2017.07	2018.08	21	−3.44	35.41	1.69	90.52
	D7	1988.06	1989.08	1990.01	20	−3.43	29.77	1.49	82.24
SM	D1	2004.03	2006.10	2010.03	74	−3.33	135.2	1.83	83.61
	D2	1985.06	1987.07	1990.07	62	−3.03	90.47	1.46	74.78
	D3	1965.05	1965.09	1967.03	23	−3.57	51.91	2.26	85.5
	D4	1999.06	2001.07	2002.03	34	−3.63	51.19	1.51	74.54
	D5	1981.10	1982.10	1984.05	32	−2.62	39.04	1.22	78.02
	D6	1971.04	1972.08	1973.06	27	−2.91	29.5	1.09	71.27
	D7	1979.10	1980.07	1981.08	23	−2.4	29.08	1.26	89.03
SW	**D1**	**1985.07**	**1987.09**	**1990.04**	**58**	**−3.95**	**123.85**	**2.14**	**79.87**
	D2	1961.09	1963.11	1964.03	31	−3.83	64.68	2.09	91.58
	D3	2008.03	2009.08	2010.08	30	−5.05	60.77	2.03	84.24
	D4	2004.04	2005.07	2005.12	21	−2.57	32.08	1.53	88.27
NM	D1	2004.04	2009.09	2011.01	82	−4.17	175.59	2.14	86.18
	D2	1977.08	1980.09	1983.05	70	−3.25	136.73	1.95	88.26
	D3	1999.11	2002.09	2003.02	40	−3.97	36.58	0.91	63.28
NW	D1	1970.1	1975.08	1983.04	121	−4.67	322.66	2.67	88.41
	D2	1961.09	1962.09	1967.06	70	−3.19	125.91	1.80	86.11
	D3	2005.06	2009.08	2009.10	53	−4.97	122.79	2.32	91.99
	D4	2017.04	2018.06	2018.12	21	−3.59	54.19	2.58	99.19

3.2.4. Spatial Characteristics

An understanding of the spatial variability of drought is significant for assessing drought hazards [62]. The spatial indices (Equations (5)–(8) and drought event number) are shown in Figure 7. The central part of the NM and the northern part of the NE had relatively large mean drought duration and MDS but relatively small mean drought frequency and drought event number, indicating that fewer drought events with longer duration and greater severity occurred in these regions. In contrast, more drought events with shorter duration and less severity occurred in the SE and SM. These results are consistent with the scPDSI results (Figure 6) in the NM, NE, SE, and SM. Figure 8 shows that the spatial patterns of the mean drought intensity and mean drought peak were different from those of the mean drought duration and mean drought severity. However, the spatial pattern of the mean drought intensity was in good agreement with that of the mean drought peak; the largest values of mean drought intensity and mean drought peak occurred in the eastern NM and western NE.

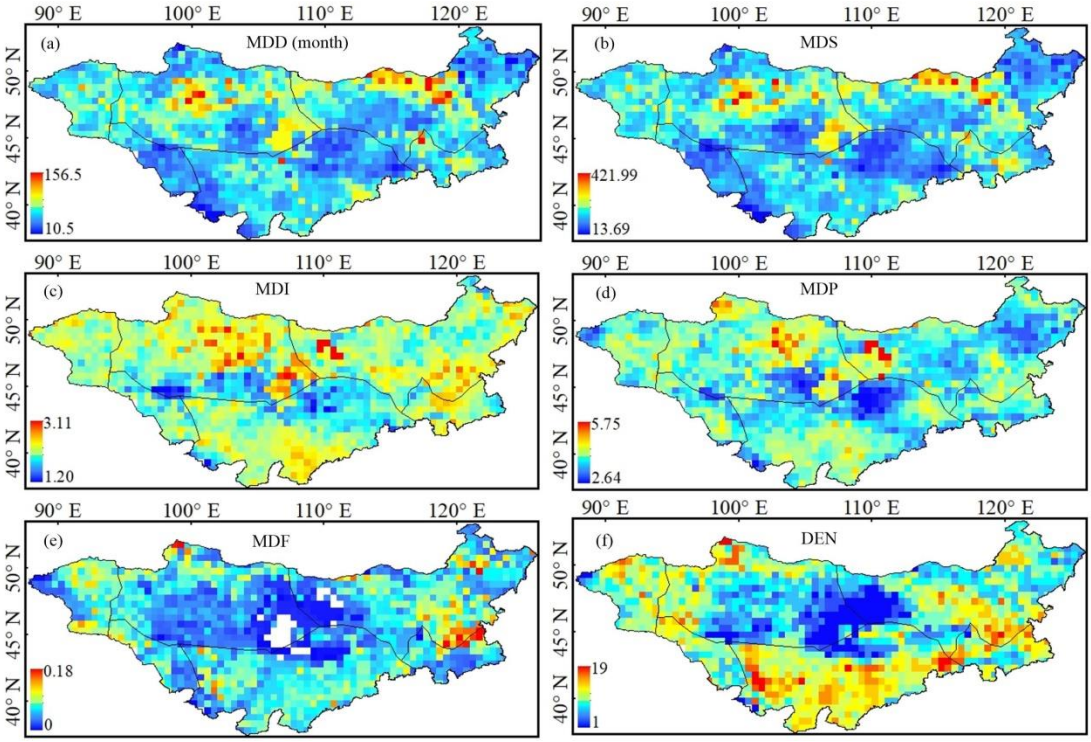

Figure 7. Spatial characteristics of drought events from 1959 to 2018. (**a**) MDD, (**b**) MDS, (**c**) MDI, (**d**) MDP, (**e**) MDF, (**f**) DEN.

Figure 8 shows the relative differences of characteristics of drought events before and after the abrupt change (1959–1995 and 1996–2018). Most areas in the MP (especially in the NW, NM, SW, and SM) had a relatively humid trend in 1996–2018 compared to the period of 1959–1995 based on the lower RMDD and RMDS values. This finding largely agrees with the results of [3]. However, some regions (i.e., the northern NE and western SE) exhibited opposite trends and larger RMDD and RMDS values. The RMDF and RDEN were higher in 1996–2018 than in 1959–1995 in the MP (especially in the NW and NM), indicating that more drought events with shorter duration and less severity occurred in these two sub-regions in 1996–2018 than in 1959–1995. Figure 8c,d show that the RMDI and RMDP values are similar in the two time periods and the positive values are observed at the junction of the NE, SM, and NM.

The study period is firstly divided into two periods (1959–1995 and 1996–2018) based on the MK change point, and then the drought frequent season significance is calculated by dividing the drought occurrence number in a given season by the number of all drought events for a given raster. For a given raster, if the ratio is larger than 50% in a given season, this raster is deemed as significance in that given season. For a given raster, if season significance cannot be found, it is showed as "Radom".

The DFSS is suitable for determining the beginning of drought events and to develop policies to mitigate drought hazards by judging the different seasons when drought events occur. Figure 9 shows the spatial distribution of the DFSS values in the periods of 1959–1995 and 1996–2018. The common feature in these two periods is that the drought events in most of the MP begin in the summer. This result is similar to the temporal distribution of "up to severe drought" described by Liu et al. [63]. Compared with 1959–1995, summer drought events increased in the west of NE, northwestern SM, and south of NM in 1996–2015.

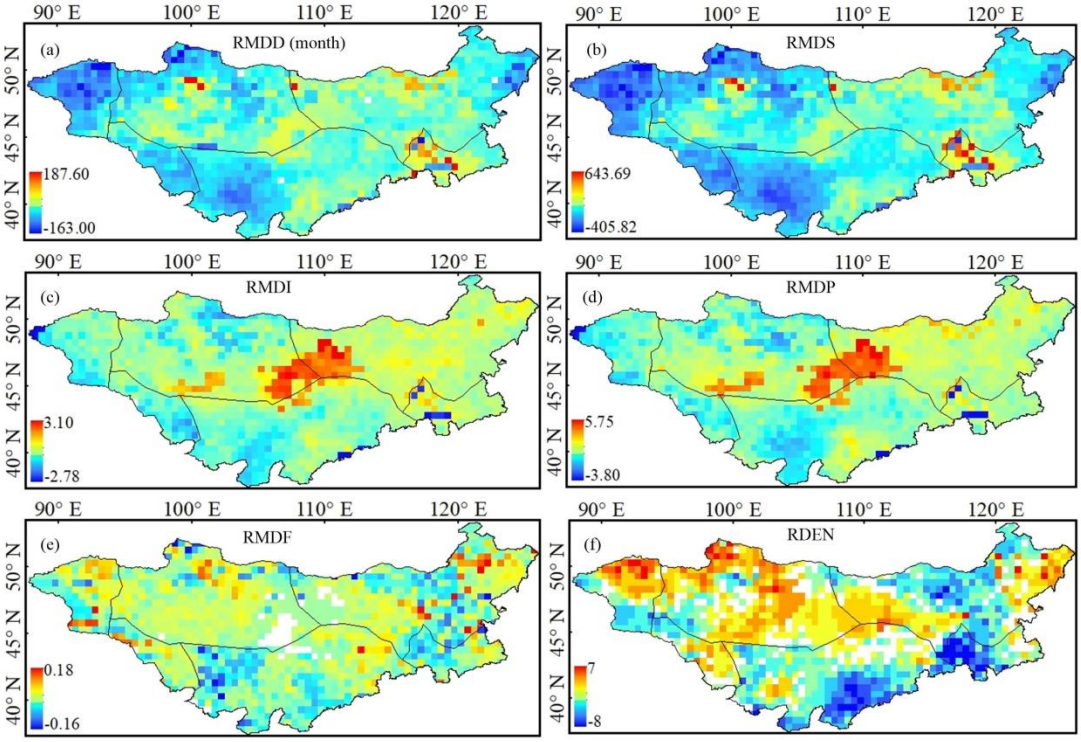

Figure 8. Spatial pattern of the relative differences in the drought events before and after the abrupt change (1959–1995 and 1996–2018). (**a**) RMDD, (**b**) RMDS, (**c**) RMDI, (**d**) RMDP, (**e**) RMDF, (**f**) RDEN.

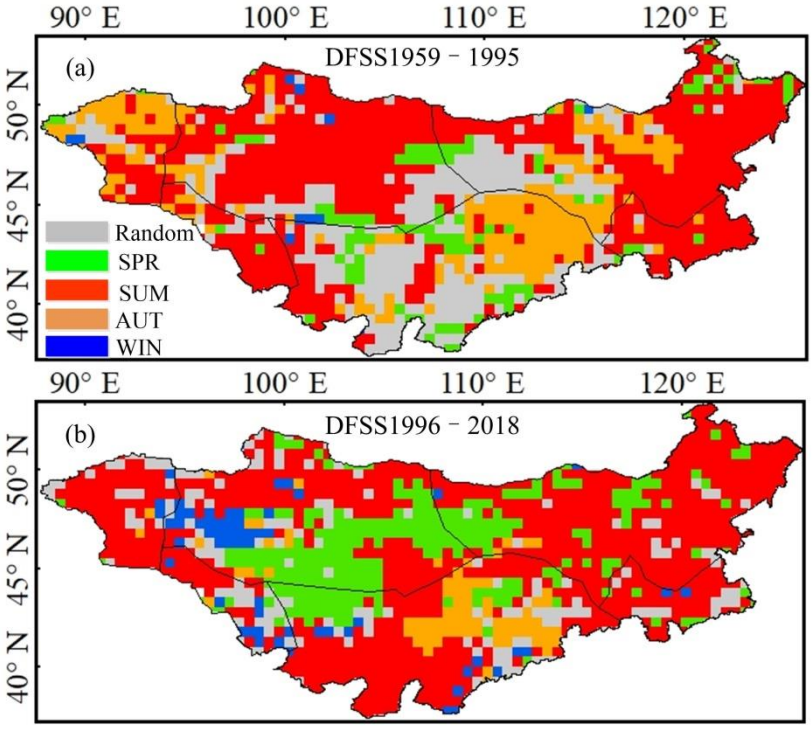

Figure 9. Spatial pattern of the DFSS of the drought events in the periods of (**a**) 1959–1995 and (**b**) 1996–2018. SPR, SUM, AUT, and WIN are spring, summer, autumn, and winter, respectively.

In general, the frequency of spring drought events exhibited an increasing trend (increase by 1.44 times), and random drought events showed a decreasing trend (decrease by 47.45%) in 1996–2018 compared with 1959–1995. This result is undesirable for agriculture in

the MP because agricultural water is urgently needed in spring. Compared with 1959–1995, spring drought events have increased in the NM and random drought events decreased in the NM and SM between 1996 and 2015.

Compared with 1959–1995, autumn drought events mainly decrease in NW and the central region of NE from 1996 to 2015; winter events mainly increase west of NM in 1996–2015.

Figure 10 shows the drought trend based on the MK test and Sen's slope at a 0.05 significance level in the two periods (1959–1995 and 1996–2018). As shown in Figure 8a, the MP exhibited in most areas (88.77%) a significantly dry trend in 1959–2018. Almost the entire NE and SE area experienced a significantly dry trend, and a wet trend occurred in the NW and SE. The area with a significantly wet trend accounted for 60.23% of the NW.

In contrast to the trends in 1959–2018, the spatial patterns of the drought trend were complex in 1996–2018. It is worth noting that there are larger areas with a wetting trend (42.37%) and smaller areas with a drought trend (58.63%). The largest proportions of areas with a significantly dry trend and significantly wet trend occurred in the NE and NM, accounting for 54.66% and 36.02% of the sub-regions. However, the mixed patterns also indicated an overall drying trend in the MP between 1996 and 2018. In addition, it should be noted that the SM, NM, and SE exhibited trends from dry in 1959–2018 to wet in 1996–2018; the proportions of areas with a wet trend in the three sub-regions changed from 20.95% to 53.54%, from 2.56% to 52.83%, and from 0% to 56.10%, respectively.

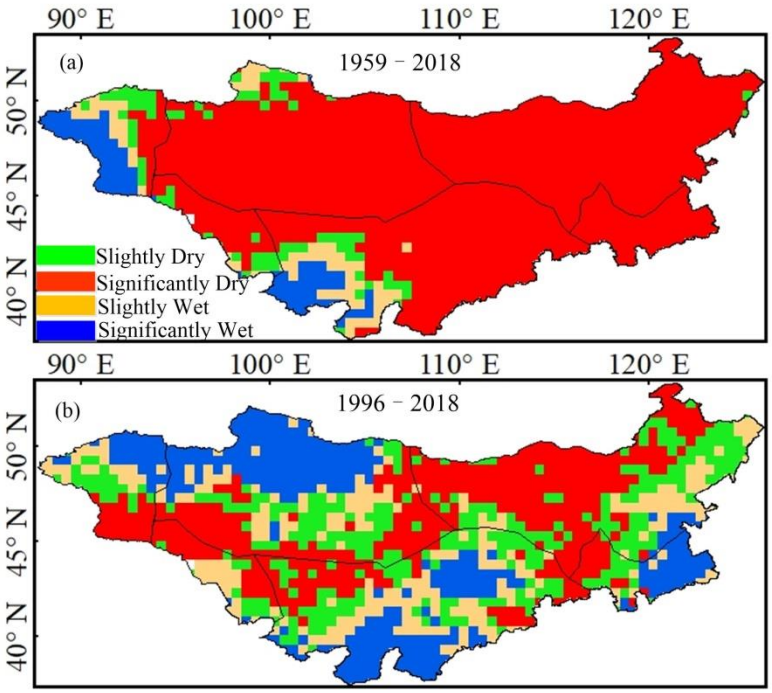

Figure 10. Spatial trend of drought in the MP based on (**a**) Sen's slope and the (**b**) MK trend test.

3.2.5. Drought Periodicity

Wavelet analysis is used to analyze variations in power spectra components within a time series by decomposing it within the time frequency space, which can describe the variability of drought patterns and represent the contribution of each period/scale to the overall variance [64]. The wavelet transform breaks up a signal into scaled versions of a wavelet function and expresses a time series in a three-dimensional space [65]—time (x), scale/frequency (y), and power (z)—thereby enabling one to explore the periodic component of drought time series. The power spectrum of the continuous wavelet transform has been used to investigate the physical mechanisms underlying the evolution of drought events [64]. Figure 11 shows the regional wavelet power spectra based on the monthly averaged scPDSI values. The sub-regions had drought periodicities in the range of

10–64 months and the significant power patterns differed for the six sub-regions. Moreover, there were very few high-power periodicities (less than 16 months) in the sub-regions. Additionally, the power spectra exhibit considerable differences for the sub-regions.

In the SE, a periodicity of 30–64 months with increasing amplitude was observed from 1965 to 1974 and a periodicity of 8–62 months with decreasing amplitude occurred from 1991 to 2003. In the NE, the wavelet power with significant values at a level of 0.05 was observed in 1985–2003 with periodicities of 10–64 months. Unlike the other sub-regions, only one area of significant wavelet power with 30–64 months periodicity and increasing amplitude was observed around 1970. The power spectra were similar in the SW, NW, and NM; the periodicities were in the range of 16–35 months, but the time periods were different. Although he scPDSI in the NM and NW exhibited considerable decadal variability (around 128-month) in 1970–2010 and 1990–2010, these values were not significant at the level of 0.05. It is noteworthy that only one area of periodicity with about 128 months was identified in the SW between 1982 and 1990. In comparison, the NE, SW, NM, and NW showed decreasing periodicity after 2000.

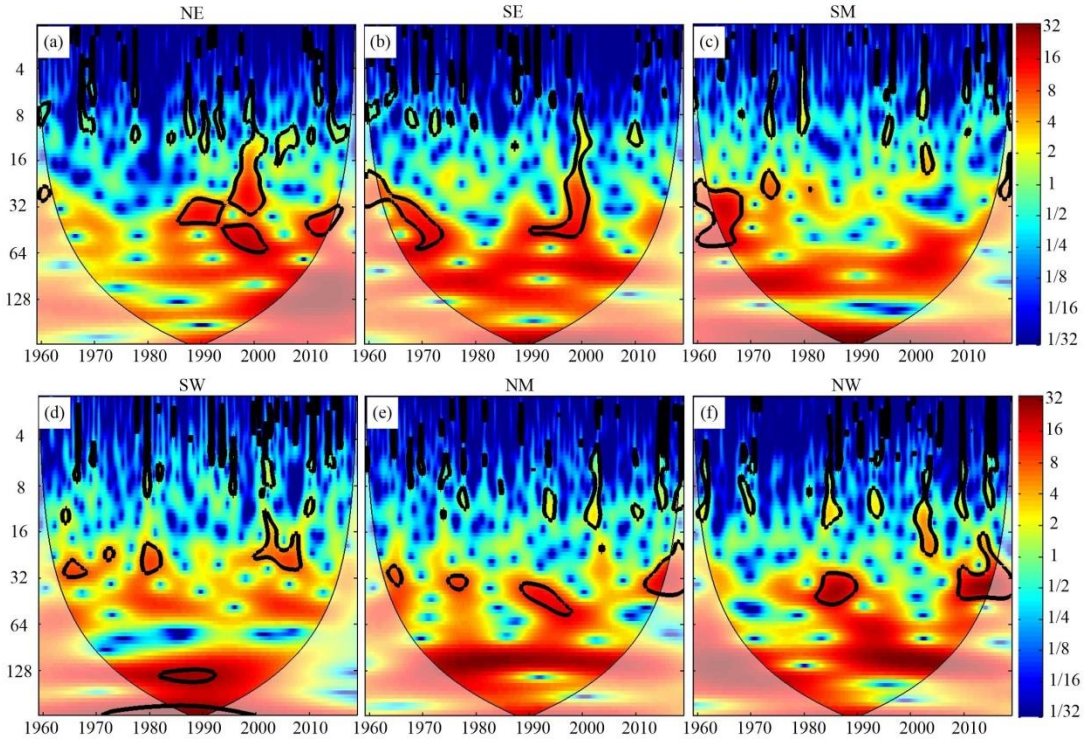

Figure 11. The power spectra of the continuous wavelet transform (CWT) of the monthly averaged scPDSI in the six sub-regions between 1959 and 2018. The change from red to blue indicates a decrease in the wavelet power. The cone of influence (COI) is represented by the light shade. The black contour is the local wavelet power relative to red noise with a 0.05 significance level threshold. (**a**) NE, (**b**) SE, (**c**) SM, (**d**) SW, (**e**) NM, (**f**) NW.

3.3. Influence of Climate Teleconnection on Regional Drought Variability

Wang et al. [66] reported that an investigation of the influence of climate patterns on regional drought evolution provides information on regional drought occurrence mechanisms and a link between atmospheric circulation and regional drought variation. The wavelet coherence patterns between the Northern Arctic Oscillation, Arctic Oscillation, Pacific Decadal Oscillation (PDO), and Niño 3.4 and the mean scPDSI in the sub-regions are depicted in Figure 12.

A significantly negative coherence with 25–50 months between the Northern Arctic Oscillation and scPDSI in 1978–1993 was identified in the NE; a Northern Arctic Oscillation leading coherence with 70–140 months was also observed between 1983 and 2010. This result indicated that the Northern Arctic Oscillation had an important influence on the drought evolution in the NE. The Arctic Oscillation had a similar anti-phase relationship with the drought evolution in the SE in 1983–1992 and the opposite in-phase coherence with 10–25 months occurred after 2010. In-phase coherence with a period of 32–52 months was found for the Pacific Decadal Oscillation from 1970 to 2000 in the SE. For the Niño 3.4 in the NE, there were two anti-phase coherences with periods of 34–60 months and 8–20 months in 1967–1985 and in 1982–1985, respectively, and in-phase coherence with a period of 16–32 months in 1995–2010.

In the SE and SM, there were significant coherence patterns with an anti-phase relationship with 60–120 months during 1966–1990 and 1966–1982, which means that the Arctic Oscillation had strong influences on the drought variation in the two sub-regions. In particular, a significant Arctic Oscillation leading coherence around 128 months was detected in 1983–1995. Similar to the SE and SM, in the SW, the Arctic Oscillation also showed a significant influence on drought variation but had a relationship at the decadal scale (128–256 months) in 1980–2000. The strong influence, which only occurred prior to 2000, may indicate a weakening effect of the Arctic Oscillation in the SE, SW, and SM.

The coherence at the decadal scale (>80 months) in the NM indicates that regional drought variations in these two sub-regions were primarily influenced by the Arctic Oscillation and Pacific Decadal Oscillation. However, the coherence patterns were different for the Arctic Oscillation and PDO. In the NM, significant coherence at 80–100 months was detected from 1970 to 1990. However, coherence at the 80–130 month scale was observed in 1974–2007. The Pacific Decadal Oscillation has increasing effect on the drought variance in the NM and there was an influence or an edge effect after 2007.

In the NW, the Pacific Decadal Oscillation had the highest correlation with the average scPDSI in the range of 8–128 months. Several significant coherence patterns of 12–32 months were identified in the following periods: 1970–1973, 1978–1982, 1992–1996, and 2008–2011. Additionally, a coherence pattern of 34–64 months was also found for 1981 to 2000. Similar to the effect of the Pacific Decadal Oscillation in the NM, the Pacific Decadal Oscillation also exhibited an increase in the coherence of 110–140 months after 1990 and there was an influence of an edge effect after 2008.

Although there were significant differences in the coherence patterns between the six sub-regions, some general conclusions can be made. The Arctic Oscillation exhibited significant correlations with the scPDSI in the southern sub-regions (including the SE, SM, and SW); the Pacific Decadal Oscillation showed the highest correlations with drought evolution in the northern sub-regions (including the NE, NM, and NW). NINO34 had an important impact on drought variation in the northern MP (the NE, NM, and NW) at the 16–64 month scale. The Northern Arctic Oscillation had less influence on drought variation in the NE, NM, NW, SE, and SW despite significant coherence patterns at the decadal scale (70–140 months) in the NE.

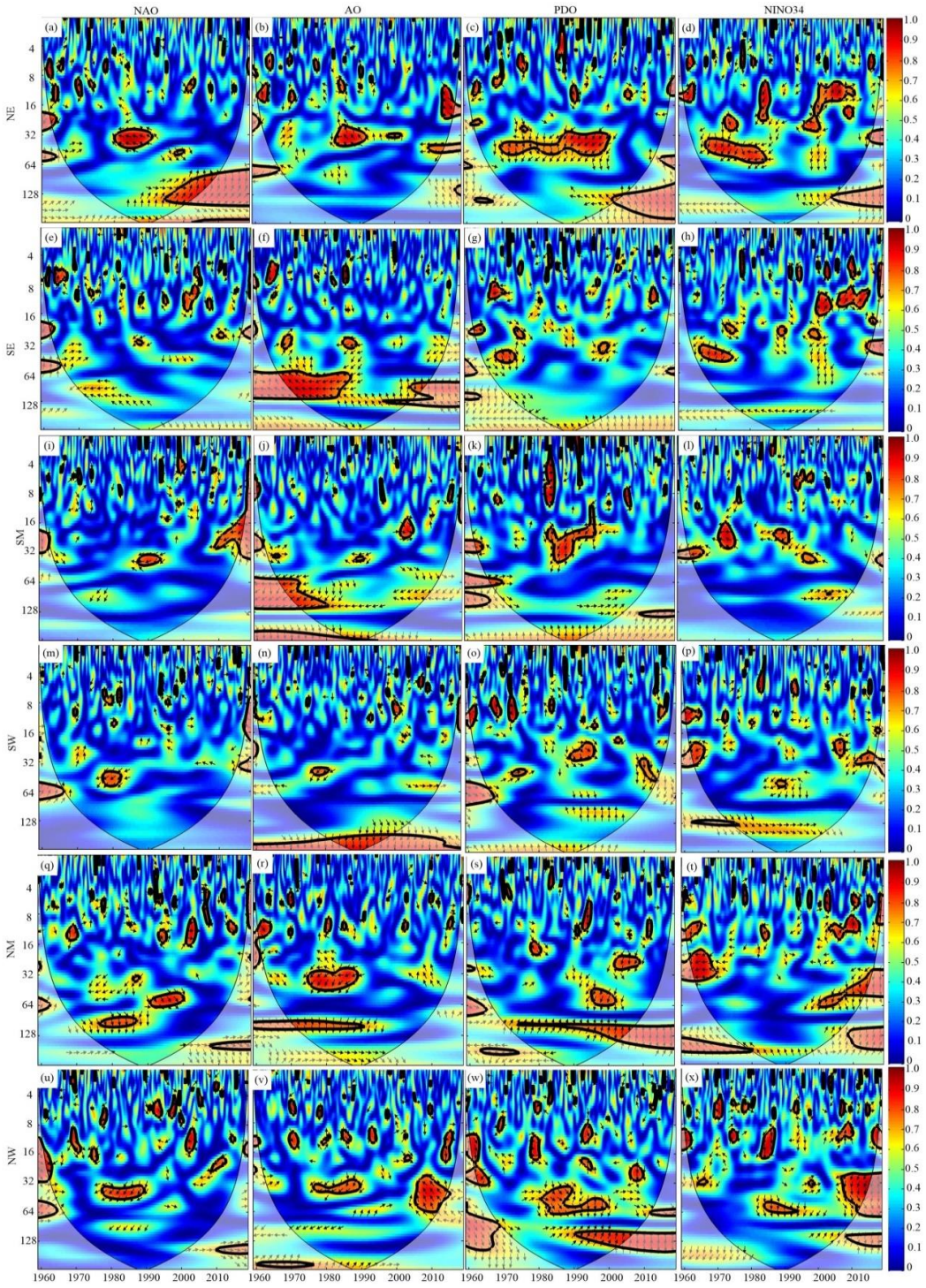

Figure 12. Wavelet coherence between the average scPDSI and four climate indices in the six subregions. Red denotes higher and blue denotes lower wavelet coherence values. The cone of influence is indicated by the light shade. The black contour is the local wavelet power relative to red noise with a 0.05 significance level threshold. The black arrows represent the phase condition.

4. Discussion

This study systematically analyzed the spatiotemporal evolution of drought characteristics in the MP between 1959 and 2018 based on the scPDSI. The results of this study provide references for regional water resources planning and agricultural production in the MP.

Several studies have investigated drought evolution in the MP. Narisu et al. [67], Cao et al. [27], and Tong et al. [3] used the PDSI, temperature vegetation dryness index (TVDI), and SPEI, respectively, to analyze the spatial and temporal variation of meteorological drought in the MP. Generally, the results of these studies indicate an increasing drought trend in the MP since the 1980s. Although previous study periods were shorter than the period used in this study, the increase in arid trends in the MP is consistent with previous findings. Moreover, studies have shown that precipitation has decreased and temperatures have increased in the MP [68,69]; this has been accompanied by intensified aridification in the MP and Inner Mongolia [22]. Figure S2 shows the spatial and temporal trends of annual precipitation and mean temperatures in the MP from 1959 to 2018 based on the CRU data. An increasing trend in temperatures was observed in the MP. The decrease in precipitation and increase in temperature in the north-central part of the MP resulted in a significant increase in drought events. As temperatures increased, an increase in the precipitation in the SW and NW alleviated local drought conditions. In general, drought intensification in the MP is mainly attributed to increased temperatures and decreased precipitation. In addition, we found that there were more areas with wetting trends and fewer areas with drought events in 1996–2018 than in 1959–1995. This was in agreement with the results of another study [70], which found that surface water resources in the MP, including lake areas and lake numbers, had recovered since 2009.

What sets this study apart from previous drought studies in the MP is the longer study period (1959–2018) and the spatiotemporal analysis of the characteristics (i.e., the DD, DP, DS, DI, and DA) of drought events at the sub-regional scale. This analysis method has several advantages over the methods used in previous studies. It provides an indication of drought vulnerability to establish drought adaptation strategies, as well as insights into the structure and mitigation of drought events [71,72]. The analysis of the characteristics of drought events provides a deeper understanding of drought compared to previous studies that focused only on drought indices. However, this may lead to different conclusions due to different definitions of drought events.

The wavelet coherence was used in this study to investigate the influences of large-scale climate patterns on drought evolution at the sub-regional level. There were significant differences in the coherence patterns for the six sub-regions, which was consistent with results reported for other arid and semi-arid regions in Asia [26]. Additionally, this study showed that the Arctic Oscillation and NINO34 had significant effects on the occurrence of drought events in the MP; this was attributed partly to the strong negative (positive) influence on precipitation (temperature) extremes in Inner Mongolia [35]. The significant impact of the Pacific Decadal Oscillation on the occurrence of drought events in the MP may be related to summer wind speeds [34].

5. Conclusions

A systematical analysis was conducted of the spatiotemporal changes in the characteristics of drought events (duration, frequency, severity, intensity, peak, and starting season) from 1959 to 2018. The main conclusions are as follows:

(1) The number of the most severe drought events was not significantly different for the two time periods of 1959–1995 and 1996–2018. Drought events occurred predominantly in the NW, SW, SM, SE, and NE in 1960–1965; in the SE, SW, NM, and NW in 1970–1985; and in all sub-regions in 2000–2012.

(2) The patterns of the drought characteristics exhibited considerable variations in the Mongolian Plateau. The central part of the NM and the northern part of the NE has relatively larger mean drought duration and mean drought severity but relatively smaller mean drought frequency and less EN. In contrast, more drought events with shorter duration and less severity occurred in the SE and SM.

(3) Most of the area in the Mongolian Plateau experienced a relatively humidity trend in 1996–2018, unlike in 1959–1995. The results of mean drought frequency and drought

event number indicated that there were more drought events with shorter duration and less severity in 1996–2018 than in 1959–1995.

(4) The frequency of spring drought events showed an increasing trend and random drought events exhibited a decreasing trend in 1996–2018 in contrast to the drought events in 1959–1995 (especially in the NM).

(5) The drought periodicities in the six sub-regions were in the range of 10–64 months and there were significant differences in the wavelet power patterns in the six sub-regions.

(6) The Arctic Oscillation was significantly correlated with the scPDSI in the southern sub-regions (including the SE, SM, and SW); the Pacific Decadal Oscillation had the largest influence on the drought evolution in the northern sub-regions (including the NE, NM, and NW).

Supplementary Materials: The following supporting information can be downloaded at: https://www.mdpi.com/article/10.3390/w14020230/s1, Figure S1: History area evolution of drought events at different drought ranks from 1959 to 2018. The green line means the 20-year smoothed line based on the LOESS; Figure S2: The MK significant values at a 0.05 significance threshold in annual precipitation (a) and annual mean temperature (b) over Mongolian Plateau during 1959–2018; Table S1: Teleconnection indices used in this study with their full name, time period and source; Table S2: Variance contributions of the un-rotated and rotated components based on monthly scPDSI; Table S3: Drought trend based on MK and Sen's slope

Author Contributions: Conceptualization, Y.H. and H.Z.; methodology, Y.H. and H.Z.; software, B.L.; formal analysis, B.L.; investigation, X.Y.; writing—original draft preparation, Y.H.; writing—review and editing, H.Z.; visualization, Y.H.; supervision, H.Z.; project administration, Bowen Liu; funding acquisition, Y.H. All authors have read and agreed to the published version of the manuscript.

Funding: This research received no external funding.

Institutional Review Board Statement: Not applicable.

Informed Consent Statement: Not applicable.

Data Availability Statement: Not applicable.

Acknowledgments: This study was financially funded by the Beijing Key Laboratory of Urban Spatial Information Engineering (grant no. 20210214).

Conflicts of Interest: The authors declare no conflict of interest.

References

1. Feng, S.F.; Hao, Z.C.; Zhang, X.; Hao, F.H. Probabilistic evaluation of the impact of compound dry-hot events on global maize yields. *Sci. Total Environ.* **2019**, *689*, 1228–1234. [CrossRef]
2. Ozelkan, E.; Chen, G.; Ustundag, B.B. Multiscale object-based drought monitoring and comparison in rainfed and irrigated agriculture from Landsat 8 OLI imagery. *Int. J. Appl. Earth Obs. Geoinf.* **2015**, *44*, 159–170. [CrossRef]
3. Tong, S.Q.; Lai, Q.; Zhang, J.Q.; Bao, Y.H.; Lusi, A.; Ma, Q.Y.; Li, X.Q.; Zhang, F. Spatiotemporal drought variability on the Mongolian Plateau from 1980–2014 based on the SPEI-PM, intensity analysis and Hurst exponent. *Sci. Total Environ.* **2018**, *615*, 1557–1565. [CrossRef] [PubMed]
4. Li, X.M.; Yang, W.F.; Yang, X.L.; Li, Y.L. Sensitivity analysis of drought indices used in Shaanxi Province. *J. Desert Res.* **2009**, *29*, 342–347.
5. Giannakopoulos, C.; Sager, P.L.; Bindi, M.; Moriondo, M.; Kostopoulou, E.; Goodess, C.M. Climatic changes and associated impacts in the Mediterranean resulting from a 2 °C global warming. *Glob. Planet. Chang.* **2009**, *68*, 209–224. [CrossRef]
6. Guo, S.J. The meteorological disaster risk assessment based on the diffusion mechanism. *J. Risk Anal. Crisis Res.* **2012**, *2*, 124–130. [CrossRef]
7. Dai, A. Drought under global warming: A review. *WIREs Clim. Change* **2011**, *2*, 45–65. [CrossRef]
8. Heim, R.R. A review of twentieth-century drought indices used in the United States. *Bull. Am. Meteorol. Soc.* **2002**, *83*, 1149–1165. [CrossRef]
9. Keyantash, J.; Dracup, J.A. The quantification of drought: An evaluation of drought indices. *Bull. Am. Meteorol. Soc.* **2002**, *83*, 1167–1180. [CrossRef]
10. Palmer, W.C. *Meteorological Drought*; US Department of Commerce, Weather Bureau: Washington, DC, USA, 1965.
11. Vicente-Serrano, S.M.; Begueria, S.; Lopez-Moreno, J.I. A multiscalar drought index sensitive to global warming: The standardized precipitation evapotranspiration index. *J. Clim.* **2010**, *23*, 1696–1718. [CrossRef]

12. Mckee, T.B.; Doedken, N.J.; Kleist, J. The relationship of drought frequency and duration to time scales. In Proceedings of the 8th Conference on Applied Climatology, Anaheim, CA, USA, 17–22 January 1993; pp. 179–182.
13. Brutsaert, W. Indications of increasing land surface evaporation during the second half of the 20th century. *Geophys. Res. Lett.* **2006**, *33*, L20403. [CrossRef]
14. Alley, W.M. The Palmer drought severity index: Limitations and assumptions. *J. Clim. Appl. Meteorol.* **1984**, *23*, 1100–1109. [CrossRef]
15. Wells, N.; Goddard, S.; Hayes, M.J. A self-calibrating Palmer drought severity index. *J. Clim.* **2004**, *17*, 2335–2351. [CrossRef]
16. Leng, F.W. The recent progress of carbon cycle research in east Asian. *Prog. Biochem. Biophys.* **2011**, *38*, 1015–1019. [CrossRef]
17. Zhen, L.; Liu, J.Y.; Liu, X.L.; Wang, L.; Batkhishig, O.; Wang, Q.X. Structural change of agriculture-livestock system and affecting factors in Mongolian Plateau. *J. Arid Land Resour. Environ.* **2008**, *22*, 144–151.
18. John, R.; Chen, J.; Ouyang, Z.; Batkishig, O.; Samanta, A.; Ganguly, S.; Yuan, W.; Xiao, J. Vegetation response to extreme climate events on the Mongolian Plateau from 2000 to 2010. *Environ. Res. Lett.* **2013**, *8*, 035033. [CrossRef]
19. Wang, L.; Zhen, L.; Liu, X.L.; Batkhishig, O.; Wang, Q. Comparative studies on climate changes and influencing factors in central Mongolian Plateau region. *Geogr. Res.* **2008**, *27*, 171–180.
20. Huang, J.; Xue, Y.; Sun, S.; Zhang, J. Spatial and temporal variability of drought during 1960–2012 in Inner Mongolia, North China. *Quat. Int.* **2015**, *355*, 134–144. [CrossRef]
21. Li, R.; Tsunekawa, A.; Tsubo, M. Index-based assessment of agricultural drought in a semi-arid region of Inner Mongolia, China. *J. Arid Land* **2014**, *6*, 3–15. [CrossRef]
22. Liu, S.; Kang, W.; Wang, T. Drought variability in inner Mongolia of northern China during 1960–2013 based on standardized precipitation evapotranspiration index. *Environ. Earth Sci.* **2016**, *75*, 145. [CrossRef]
23. Shen, Z.X.; Zhang, Q.; Singh, V.P.; Sun, P.; Song, C.Q.; Yu, H.Q. Agricultural drought monitoring across Inner Mongolia, China: Model development, spatiotemporal patterns and impacts. *J. Hydrol.* **2019**, *571*, 793–804. [CrossRef]
24. Wang, Y.; Liu, G.; Guo, E. Spatial distribution and temporal variation of drought in Inner Mongolia during 1901–2014 using Standardized Precipitation Evapotranspiration Index. *Sci. Total Environ.* **2019**, *654*, 850–862. [CrossRef] [PubMed]
25. Cheng, C.H.; Nnadi, F.; Liou, Y.A. A regional land use drought index for Florida. *Remote Sens.* **2015**, *7*, 17149–17167. [CrossRef]
26. Guo, H.; Bao, A.M.; Liu, T.; Jiapaer, G.; Ndayisab, F.; Jiang, L.L.; Kurban, A.; Maeyer, P.D. Spatial and temporal characteristics of droughts in Central Asia during 1966–2015. *Sci. Total Environ.* **2018**, *624*, 1523–1538. [CrossRef] [PubMed]
27. Cao, X.M.; Feng, Y.M.; Wang, J.L.; Gao, Z.Q.; Ning, J.C.; Gao, W. The study of the spatio-temporal changes of drought in the Mongolian Plateau in 40 years based on TVDI. *Proc. SPIE* **2014**, *9221*, 92210X-1.
28. Bao, G.; Chen, J.Q.; Chopping, M.; Bao, Y.H.; Bayarsaikhan, S.; Dorjsuren, A.; Tuya, A.; Jirigala, B.; Qing, Z.H. Dynamics of net primary productivity on the Mongolian Plateau: Joint regulations of phenology and drought. *Int. J. Appl. Earth. Obs. Geoinf.* **2019**, *81*, 85–97. [CrossRef]
29. Wei, Y.; Zhen, L.; Batkhishig, O.; Liu, X.; Fen, L.I.; Yang, L. Empirical study on consumption of ecosystem services and its spatial differences over Mongolian Plateau. *Res. Sci.* **2009**, *31*, 1677–1684.
30. Zhang, X.; Hu, Y.; Zhuang, D.; Qi, Y.Q.; Ma, X. NDVI spatial pattern and its differentiation on the Mongolian Plateau. *J. Geogr. Sci.* **2009**, *19*, 403–415. [CrossRef]
31. Miao, L.J.; Luan, Y.B.; Luo, X.Z.; Liu, Q.; Moore, J.C.; Nath, R.; He, B.; Zhu, F.; Cui, X.F. Analysis of the Phenology in the Mongolian Plateau by Inter-Comparison of Global Vegetation Datasets. *Remote Sens.* **2013**, *5*, 5193–5208. [CrossRef]
32. Mitchell, T.D.; Jones, P.D. An improved method of constructing a database of monthly climate observations and associated high-resolution grids. *Int. J. Climatol.* **2005**, *25*, 693–712. [CrossRef]
33. Jones, P.D.; Harpham, C.; Harris, I.; Goodess, C.M.; Burton, A.; Centella-Artola, A.; Taylor, M.A.; Bezanilla-Morlot, A.; Campbell, J.D.; Stephenson, T.S.; et al. Long-term trends in precipitation and temperature across the Caribbean. *Int. J. Clim.* **2015**, *36*, 3314–3333. [CrossRef]
34. Yu, L.J.; Zhong, S.Y.; Bian, X.D.; Heilman, W.E. Climatology and trend of wind power resources in China and its surrounding regions: A revisit using Climate Forecast System Reanalysis data. *Int. J. Climatol.* **2016**, *36*, 2173–2188. [CrossRef]
35. Tong, S.Q.; Li, X.Q.; Zhang, J.Q.; Bao, Y.H.; Bao, Y.B.; Na, L.; Si, A.L. Spatial and temporal variability in extreme temperature and precipitation events in Inner Mongolia (China) during 1960–2017. *Sci. Total Environ.* **2019**, *649*, 75–89. [CrossRef]
36. Choi, J.W.; Kim, I.G.; Kim, J.Y.; Kim, B.J.; Parka, C.H.; Kim, D.W. The assessment of droughts in Northern China and Mongolian areas using PDSI and relevant large-scale environments. *Int. J. Climatol.* **2016**, *36*, 3259–3269. [CrossRef]
37. Wang, H.J.; Chen, Y.N.; Pan, Y.P.; Li, W.H. Spatial and temporal variability of drought in the arid region of China and its relationships to teleconnection indices. *J. Hydrol.* **2015**, *523*, 283–296. [CrossRef]
38. Chen, J.; John, R.; Zhang, Y.Q.; Shao, C.L.; Brown, D.G.; Batkhishig, O.; Amarjargal, A.; Ouyang, Z.T.; Dong, G.; Wang, D.; et al. Divergences of Two Coupled Human and Natural Systems on the Mongolian Plateau. *BioScience* **2015**, *65*, 559–570. [CrossRef]
39. Huang, S.Z.; Huang, Q.; Chang, J.X.; Leng, G.Y.; Xing, L. The response of agricultural drought to meteorological drought and the influencing factors: A case study in the Wei River Basin, China. *Agric. Water Manag.* **2015**, *159*, 45–54. [CrossRef]
40. Liu, X.; Wang, S.; Zhou, Y.; Wang, F.; Li, W.; Liu, W. Regionalization and Spatiotemporal Variation of Drought in China Based on Standardized Precipitation Evapotranspiration Index (1961–2013). *Adv. Meteorol.* **2015**, *2015*, 1–18. [CrossRef]
41. Montaseri, M.; Amirataee, B. Comprehensive stochastic assessment of meteorological drought indices. *Int. J. Climatol.* **2017**, *37*, 998–1013. [CrossRef]

42. Gregor, M. *Surface and Groundwater Quality Changes in Periods of Water Scarcity*; Springer Science & Business Media: Berlin/Heidelberg, Germany, 2012.
43. Venturas, M.D.; MacKinnon, E.D.; Dario, H.L.; Jacobsen, A.L.; Pratt, R.B.; Davis, S.D. Chaparral shrub hydraulic traits, size, and life history types relate to species mortality during California's historic drought of 2014. *PLoS ONE* **2016**, *11*, e0159145. [CrossRef]
44. Liu, Y.W.; Liu, Y.B.; Wang, W. Inter-comparison of satellite-retrieved and Global Land Data Assimilation System-simulated soil moisture datasets for global drought analysis. *Remote Sens. Environ.* **2019**, *220*, 1–18. [CrossRef]
45. Raziei, T.; Saghafian, B.; Paulo, A.A.; Pereira, L.S.; Bordi, I. Spatial patterns and temporal variability of drought in Western Iran. *Water Resour. Manag.* **2008**, *23*, 439–455. [CrossRef]
46. North, G.R.; Bell, T.L.; Cahalan, R.F.; Moeng, F.J. Sampling errors in the estimation of empirical orthogonal functions. *Mon. Weather Rev.* **1982**, *110*, 699–706. [CrossRef]
47. Kendall, M.G. *Rank Correlation Methods*; Charles Griffin: London, UK, 1990.
48. Mann, H.B. Nonparametric tests against trend. *Econometrica* **1945**, *13*, 245–259. [CrossRef]
49. Sen, P.K. Estimates of the regression coefficient based on Kendall's tau. *Am. Stat. Assoc.* **1968**, *63*, 1379. [CrossRef]
50. Salehi, S.; Dehghani, M.; Mortazavi, S.M.; Singh, V.P. Trend analysis and change point detection of seasonal and annual precipitation in Iran. *Int. J. Clim.* **2020**, *40*, 308–323. [CrossRef]
51. Wang, Y.; Zhang, T.; Chen, X.; Li, J.; Feng, P. Spatial and temporal characteristics of droughts in Luanhe River basin, China. *Theor. Appl. Climatol.* **2018**, *131*, 1369–1385. [CrossRef]
52. Smadi, M.M.; Zghoul, A. A sudden change in rainfall characteristics in Amman, Jordan during the mid 1950s. *Am. J. Environ. Sci.* **2006**, *2*, 84–91. [CrossRef]
53. Da Silva, R.M.; Santos, C.A.; Moreira, M.; Corte-Real, J.; Silva, V.C.; Medeiros, I.C. Rainfall and river flow trends using Mann–Kendall and Sen's slope estimator statistical tests in the Cobres River basin. *Nat. Hazards* **2015**, *77*, 1205–1221. [CrossRef]
54. Joshi, N.; Gupta, D.; Suryavanshi, S.; Adamowski, J.; Madramootoo, C.A. Analysis of trends and dominant periodicities in drought variables in India: A wavelet transform based approach. *Atmos. Res.* **2016**, *182*, 200–220. [CrossRef]
55. Grinsted, A.; Moore, J.C.; Jevrejeva, S. Application of the cross wavelet transform and wavelet coherence to geophysical time series. *Nonlinear Process Geophys.* **2004**, *11*, 561–566. [CrossRef]
56. Maraun, D.; Kurths, J. Cross wavelet analysis: Significance testing and pitfalls. *Nonlinear Process Geophys.* **2004**, *11*, 505–514. [CrossRef]
57. Cleveland, W.S.; Devlin, S.J. Locally weighted regression: An approach to regression analysis by local fitting. *J. Am. Stat. Assoc.* **1988**, *83*, 596–610. [CrossRef]
58. Fernández-Duque, B.; Pérez, I.A.; Ángeles García, M.; Pardo, N.; Luisa Sánchez, M. Local regressions for decomposing CO_2 and CH4 time-series in a semi-arid ecosystem. *Atmos. Pollut. Res.* **2020**, *11*, 213–223. [CrossRef]
59. Marchetto, A.; Rogora, M.; Arisci, S. Trend analysis of atmospheric deposition data: A comparison of statistical approaches. *Atmos. Environ.* **2013**, *64*, 95–102. [CrossRef]
60. Pettitt, A.N. A Non-Parametric Approach to the Change-Point Problem. *J. R. Stat. Soc. Ser. C Appl. Stat.* **1979**, *28*, 126. [CrossRef]
61. Quiring, S.M.; Goodrich, G.B. Nature and causes of the 2002 to 2004 drought in the southwestern United States compared with the historic 1953 to 1957 drought. *Clim. Res.* **2008**, *36*, 41–52. [CrossRef]
62. Andreadis, K.M.; Clark, E.A.; Wood, A.W.; Hamlet, A.F.; Lettenmaier, D.P. Twentieth century drought in the conterminous United States. *J. Hydrometeorol.* **2005**, *6*, 985–1001. [CrossRef]
63. Liu, Z.F.; Yao, Z.J.; Huang, H.Q.; Batjav, B.; Wang, R. Evaluation of Extreme Cold and Drought over the Mongolian Plateau. *Water* **2019**, *11*, 74. [CrossRef]
64. Zeleke, T.; Giorgi, F.; Diro, G.; Zaitchik, B. Trend and periodicity of drought over Ethiopia. *Int. J. Clim.* **2017**, *37*, 4733–4748. [CrossRef]
65. Torrence, C.; Compo, G. A practical guide to wavelet analysis. *Bull. Am. Meteorol. Soc.* **1998**, *79*, 61–78. [CrossRef]
66. Wang, H.J.; Chen, Y.N.; Li, W.H. Characteristics in streamflow and extremes in the Tarim River, China: Trends, distribution and climate linkage. *Int. J. Clim.* **2014**, *35*, 761–776. [CrossRef]
67. Narisu, N.; Bao, Y.; Yushan, B. Drought Temporal Variation Characteristics Analysis based on the PDSI Data in Mongolian Plateau. *Adv. Intell. Syst. Res.* **2016**, *128*, 843–848.
68. Li, W.Y.; Qian, Z.A. Temporal and spatial feature analyses of winter and summer surface air temperature in CMASA, part (1): January. *Plateau Meteorol.* **2005**, *24*, 889–897.
69. Yatagai, A.; Yasunari, T. Interannual variations of summer precipitation in the arid/semi-arid regions in China and Mongolia: Their regionality and relation to the Asian summer monsoon. *J. Meteorol. Soc. Jpn.* **1995**, *73*, 909–923. [CrossRef]
70. Zhou, Y.; Dong, J.W.; Xiao, X.M.; Liu, R.G.; Zou, Z.H.; Zhao, G.S.; Ge, Q.S. Continuous monitoring of lake dynamics on theMongolian Plateau using all available Landsat imagery and Google Earth Engine. *Sci. Total Environ.* **2019**, *589*, 366–380. [CrossRef]
71. Guo, H.; Bao, A.M.; Ndayisaba, F.; Liu, T.; Jiapaer, G.; Attia, M.; El-Tantawi, A.M.; De Maeyer, P. Space-time characterization of drought events and their impacts on vegetation in Central Asia. *J. Hydrol.* **2018**, *564*, 1165–1178. [CrossRef]
72. Xu, K.; Yang, D.W.; Yang, H.B.; Li, Z.; Qin, Y.; Shen, Y. Spatio-temporal variation of drought in China during 1961–2012: A climatic perspective. *J. Hydrol.* **2015**, *526*, 253–264. [CrossRef]